Bull. Chem. Soc. Jpn., **68**, 1105—1114(1995)

Headline Articles

Di(phenoxo)-bridged Dinuclear Mn_2(II,II) and Mn_2(II,III) Complexes of Macrocyclic Ligands: Structure, Properties, and Catalase-Like Function

Hisae Wada, Ken-ichiro Motoda, Masaaki Ohba, Hiroshi Sakiyama, Naohide Matsumoto, and Hisashi Ōkawa*

Department of Chemistry, Faculty of Science, Kyushu University, Hakozaki 6-10-1, Higashi-ku, Fukuoka 812

(Received November 21, 1994)

Dinuclear Mn_2(II,II) complexes $[Mn_2(L^{m,n})(RCOO)_2]$ ((m,n)=(2,3), (2,4), (3,3); R=CH_3, C_6H_5) have been prepared where $(L^{m,n})^{2-}$ denotes dinucleating macrocycles with two 2,6-bis(iminomethyl)-4-methylphenolate entities combined through two lateral chains, $-(CH_2)_m-$ and $-(CH_2)_n-$, at the imino nitrogens. The complex $[Mn_2(L^{3,3})(CH_3COO)_2]$ crystallizes in the monoclinic space group $P2_1/n$ with a=18.795(5), b=7.608(2), c=10.081(1) Å, β=92.89(2)°, V=1439.7 Å^3, and Z=2. The refinement converges with R=6.38 and R_w=9.63% based on 2727 reflections with $|F_o| \geq 3\sigma(|F_o|)$. A pair of Mn(II) ions are bridged by the two phenolic oxygens with a Mn–Mn separation of 3.367(1) Å. An acetate group coordinates bidentately to each Mn(II) to afford a six-coordinate geometry about the metal ion. The oxidation of $[Mn_2(L^{3,3})(CH_3COO)_2]$ with Br_2 forms a mixed-valence Mn_2(II,III) complex $[Mn_2(L^{3,3})(CH_3COO)Br_2]\cdot H_2O$. The Mn_2(II,II) and Mn_2(II,III) complexes show catalytic activity for decomposing H_2O_2 in DMF or DMSO. The involvement of the Mn_2(II,III)/Mn_2(II,IV) cycle in the catalytic process is inferred based on visible and ESR spectroscopic studies of the reaction mixture.

The design of functional dinuclear metal complexes is of current interest to mimic bimetallic biosites[1] and to search appropriate systems for activating simple molecules.[2] The use of dinucleating macrocyclic ligands (macrocycles hereafter) for this purpose is of great advantage because dinuclear core structures can be thermodynamically stabilized and kinetically retarded towards metal dissociation by the macrocyclic effect.[3] Further, macrocycles can provide a well-defined stereochemical environment for bound metal ions and influence their physicochemical properties.[4] Thus, properties and functions of dinuclear metal complexes can be modulated by the design of macrocycles.

The dinucleating macrocycles in Scheme 1, abbreviated as $(L^{m,n})^{2-}$ where the superscripts m and n denote the methylene numbers of the two lateral chains, have been obtained for m=n by "direct template reaction"[5] and for $m \neq n$ by "stepwise template reaction".[6—8] Those macrocycles have extensively been used for studies on homo- and heterodinuclear complexes, but the studies on manganese complexes of the macrocycles are very limited[9,10] in spite of great interest as models for dimanganese biosites such as manganese catalase (MnCAT),[11] manganese ribonucleotide reductase,[12] inorganic pyrophosphatase,[13] arginase,[14] and xylose isomerase.[15]

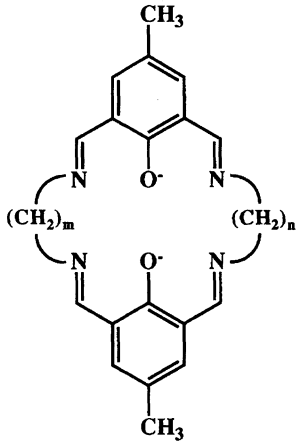

Scheme 1. Chemical structure of macrocycles $(L^{m,n})^{2-}$ ((m,n)=(2,3), (2,4), (3,3)).

In this study dinuclear Mn_2(II, II) complexes, $[Mn_2(L^{m,n})(RCOO)_2]$ ((m,n)=(2, 3), (2, 4), (3, 3);

R=CH_3, C_6H_5), have been prepared and the crystal structure of $[Mn_2(L^{3,3})(CH_3COO)_2]$ has been determined by X-ray crystallography. Further, a mixed-valence Mn$_2$(II, III) complex $[Mn_2(L^{3,3})(CH_3COO)Br_2]\cdot H_2O$ has been prepared by the oxidation of $[Mn_2(L^{3,3})(CH_3COO)_2]$ with Br_2. The CAT-like activity of the Mn$_2$(II,II) complexes for decomposing hydrogen peroxide has been studied in DMF by volumetrical measurements of evolved dioxygen, and the active species involved in the catalytic process have been examined by means of visible and ESR spectroscopies.

Experimental

Physical Measurements. Elemental analyses of C, H, and N were obtained at the Service Center of Elemental Analysis of Kyushu University. Analyses of Mn were made using a Shimadzu AA-680 Atomic Absorpsion/Flame Emission spectrophotometer. Infrared spectra were recorded on a JASCO IR-810 spectrophotometer using KBr disks. Electronic spectra were recorded on a Shimadzu MPS-2000 spectrophotometer. Molar conductances were measured with a DKK AOL-10 conductivity meter at room temperature. Magnetic susceptibilities were measured on a HOXAN HSM-D SQUID susceptometer in the temperature range of 4.2—80 K and on a Faraday balance in the range of 80—290 K. Effective magnetic moments were calculated by the equation $\mu_{eff}=2.828[\chi_A T]^{1/2}$, where diamagnetic corrections for the constituting atoms were made by the use of Pascal's constants.[16] X-Band ESR spectra were recorded on a JEOL JEX-FE3X spectrometer on frozen DMF or DMSO solution at liquid nitrogen temperature. Cyclic voltammograms were recorded on an apparatus comprising a HA-501 potentiostat/galvanostat, a HB-104 function generator, and a HF-201 coulomb/ampere-hour meter from Hokuto Denko Ltd. Measurements were carried out in DMF or DMSO solution (ca. 1×10^{-3} mol dm^{-3} (=M)) containing tetra(*n*-butyl)ammonium perchlorate (TBAP, ca. 1×10^{-1} M) as the supporting electrolyte. A three-electrode cell was used which was equipped with a glassy carbon working electrode, a platinum coil as the counter electrode, and a saturated calomel electrode as the reference (Caution! TBAP is explosive and should be handled with great care). Coulometry studies were done on the same instrument using a Pt net as the working electrode.

Preparation. 2,6-Diformyl-4-methylphenol was prepared by a modification[6] of the method of Denton and Suschitzky.[17] All the chemicals were of reagent grade and used as purchased.

$[Mn_2(L^{2,3})(CH_3COO)_2]$ (1). *N,N'*-Bis(3-formyl-5-methylsalicylidene)ethylenediaminatomanganese(II) was prepared as orange microcrystals by the reaction of 2,6-diformyl-4-methylphenol (2.0 g, 12.2 mmol), ethylenediamine (0.36 g, 6.1 mmol), and manganese(II) acetate tetrahydrate (1.5 g, 6.1 mmol) in dry methanol (100 cm^3) under anaerobic conditions. To a suspension of this complex (410 mg, 1.0 mmol) in DMF (20 cm^3) was added dropwise a DMF solution (10 cm^3) of manganese(II) acetate tetrahydrate (250 mg, 1.0 mmol) at 80 °C and the resulting red solution was stirred for one hour. Then a DMF solution (10 cm^3) of 1,3-diaminopropane (74 mg, 1.0 mmol) was added with stirring at ambient temperature to result in the precipitation of yellow microcrystals. They were separated by filtration, washed three times with absolute methanol, and dried in vacuo. The yield was 360 mg (58%). Found: C, 52.59; H, 5.00; N, 9.23; Mn, 17.53%. Calcd for $C_{27}H_{34}Mn_2N_4O_6$: C, 52.61; H, 4.91; N, 9.09; Mn, 17.82%. μ_{eff}/Mn: 5.92 μ_B at 290 K. Selected IR [ν/cm^{-1}] on KBr 1630, 1540, 1410. UV-vis [λ_{max}/nm] (ε/M^{-1} cm^{-1}) in DMF 380 (14000).

$[Mn_2(L^{2,3})(C_6H_5COO)_2]$ (2). This complex was obtained as yellow microcrystals in a way similar to that for **1**, using manganese(II) benzoate tetrahydrate (370 mg, 1.0 mmol) instead of manganese(II) acetate tetrahydrate. The yield was 360 mg (48%). Found: C, 59.91; H, 4.66; N, 7.47; Mn, 15.18%. Calcd for $C_{37}H_{34}Mn_2N_4O_6$: C, 60.01; H, 4.63; N, 7.57; Mn, 14.84%. μ_{eff}/Mn: 5.82 μ_B at 290 K. Selected IR [ν/cm^{-1}] on KBr 1640, 1540, 1400. UV-vis [λ_{max}/nm] (ε/M^{-1} cm^{-1}) in DMF 380 (15000).

$[Mn_2(L^{2,4})(C_6H_5COO)_2]$ (3). This complex was obtained as yellow microcrystals in a way similar to that for **2**, using 1,4-diaminobutane (90 mg, 1.0 mmol) instead of ethylenediamine. The yield was 200 mg (26%). Found: C, 60.71; H, 4.87; N, 7.44; Mn, 14.30%. Calcd for $C_{38}H_{36}Mn_2N_4O_6$: C, 60.49; H, 4.81; N, 7.43; Mn, 14.56%. μ_{eff}/Mn: 5.75 μ_B at 290 K. Selected IR [ν/cm^{-1}] on KBr 1640, 1620, 1535, 1410. UV-vis [λ_{max}/nm] (ε/M^{-1} cm^{-1}) in DMF 380 (14000).

$[Mn_2(L^{3,3})(CH_3COO)_2]$ (4). To a solution of 2,6-diformyl-4-methylphenol (330 mg, 2.0 mmol) and manganese(II) acetate tetrahydrate (490 mg, 2.0 mmol) in dry methanol (10 cm^3) was added a methanol solution (5 cm^3) of 1,3-diaminopropane (150 mg, 2.0 mmol). The resulting yellow solution was stirred for 1 h at ambient temperature to form lemon yellow microcrystals. They were separated by filtration, washed with dry methanol and dried in vacuo. The yield was 350 mg (55%). Found: C, 53.35; H, 5.08; N, 8.85; Mn, 17.25%. Calcd for $C_{28}H_{32}Mn_2N_4O_6$: C, 53.34; H, 5.12; N, 8.89; Mn, 17.43%. μ_{eff}/Mn: 5.92 μ_B at 290 K. Selected IR [ν/cm^{-1}] on KBr 1640, 1555, 1400. UV-vis [λ_{max}/nm] (ε/M^{-1} cm^{-1}) in DMF 380 (14000).

$[Mn_2(L^{3,3})(CH_3COO)Br_2]\cdot H_2O$ (4'). To a yellow solution of **4** (550mg, 0.88 mmol) in CH_2Cl_2 was added bromine (70 mg, 0.88 mmol), and the resulting deep green solution was stirred at ambient temperature for 3 h. The concentration of the reaction mixture to a small portion gave dark green microcrystals which were separated by suction filtration, washed with ether, and dried in vacuo. The yield was 170 mg (23%). Found: C, 42.02; H, 4.39; N, 7.45; Mn, 14.66%. Calcd for $C_{26}H_{31}Br_2Mn_2N_4O_5$: C, 41.68; H, 4.17; N, 7.48; Mn, 14.67%. μ_{eff}/2Mn: 7.74 μ_B at 290 K. Selected IR [ν/cm^{-1}] on KBr 1630, 1550, 1400. UV-vis [λ_{max}/nm] (ε/M^{-1} cm^{-1}) in DMSO 370 (11000), 570 (570).

$[Mn_2(L^{3,3})(C_6H_5COO)_2]$ (5). This complex was obtained as yellow microcrystals in a way similar to that for **4**, using manganese(II) benzoate tetrahydrate (740 mg, 2.0 mmol) instead of manganese(II) acetate tetrahydrate. The yield was 330 mg (42%). Found: C, 60.34; H, 4.77; N, 7.42; Mn, 14.22%. Calcd for $C_{38}H_{36}Mn_2N_4O_6$: C, 60.49; H, 4.81; N, 7.43; Mn, 14.56%. μ_{eff}/Mn: 5.95 μ_B at 290 K. Selected IR [ν/cm^{-1}] on KBr 1635, 1540, 1400. UV-vis [λ_{max}/nm] (ε/M^{-1} cm^{-1}) in DMF 380 (15000).

X- Ray Structural Analysis of $[Mn_2(L^{3,3})(CH_3COO)_2]$ (4). The complex **4** was dissolved in CH_2Cl_2 and the solution was layered with acetonitrile to form single crystals suitable for X-ray crystallography. A

crystal of approximate size 0.3×0.4×0.4 mm^3 was used for the X-ray diffraction study. Intensities and lattice parameters were obtained on a Rigaku Denki AFC-5 automated four-circle diffractometer, using graphite-monochromated Mo $K\alpha$ radiation (λ=0.71069 Å) at 20±1 °C. Pertinent crystallographic parameters are summarized in Table 1. Three standard reflections were monitored every 100 measurements and showed no systematic decreases in intensity. The reflection data were corrected for Lorentz and polarization factors. Corrections for absorption effects were not made.

The structure was solved by the standard heavy-atom method and refined by block-diagonal least-squares calculations. Reliability factors were defined as $R=\sum||F_o|-|F_c||/\sum|F_o|$ and $R_w=[\sum w(|F_o|-|F_c|)^2/\sum w|F_o|^2]^{1/2}$, where the weights were taken as $w=1/\sigma\ (|F_o|)^2$. The contributions for hydrogen atoms bound to carbons were introduced into the calculated positions. These hydrogen atoms were included in the structure factor calculation but not refined. The atomic scattering factors were taken from Ref. 18. All the computations were carried out on a FACOM M-1800/20 computer at the Computer Center of Kyushu University, using a local version[19] of the UNICS III[20] and ORTEP[21] programs. The final atomic coordinates are given in Table 2. Positional and thermal parameters of non-hydrogen atoms (Table S1) and hydrogen atoms (S2), anisotropic temperature factors (S3), complete list of bond distances and angles (S4), and tables of observed and calculated structure factors (S5) have been deposited as Document No. 68017 at the Office of the Editor of Bull. Chem. Soc. Jpn.

Studies on Catalase-like Activity. A closed vessel containing a dmf solution (2 cm^3) of a Mn_2(II,II) complex (5 μmol) was stirred at 0 °C on an ice-water bath. Hydrogen peroxide (10.0%, 0.5 cm^3; H_2O_2 1.45 mmol) chilled at 0 °C was injected through a silicon stopper and dioxygen evolved was measured volumetrically with a buret.

Table 1. Crystallographic Data for **4**

Formula	$C_{28}H_{32}Mn_2N_4O_6$
Color of crystal	Yellow
F. W.	630.46
Crystal dimensions/mm^3	0.3×0.4×0.4
Crystal system	Monoclinic
Space group	$P2_1/n$
a/Å	18.795(5)
b/Å	7.608(2)
c/Å	10.081(1)
β/deg	92.89(2)
V/Å^3	1439.7(5)
Z	2
D_c/g cm^{-3}	1.454
D_m/g cm^{-3}	1.450
μ(Mo $K\alpha$)/cm^{-1}	8.87
No. of reflections with $\|F_o\|\geq 3\sigma(\|F_o\|)$	2727
F(000)	1304
R[a)]	6.38
R_w[b,c)]	9.63

a) $R=\sum||F_o|-|F_c||/\sum|F_o|$. b) $R_w=[\sum w(|F_o|-|F_c|)^2/\sum[w|F_o|^2]^{1/2}$. c) $w=1/\sigma(|F_o|)^2$.

Table 2. Final Atomic Coordinates (×10^4) and B_{eq} (Å^2) of **4**

Atom	x	y	z	B_{eq}[a)]
Mn	4578.1(5)	4365(1)	6354(1)	2.2
O1	5432(2)	6035(6)	5755(4)	2.6
O2	3741(3)	6234(8)	6406(6)	4.9
O3	3696(4)	4601(11)	8167(7)	6.5
N1	5323(3)	3872(8)	8076(5)	2.8
N2	4241(3)	1603(7)	6312(5)	2.8
C1	5887(3)	6939(8)	6492(6)	2.3
C2	6203(3)	8505(9)	5999(6)	2.6
C3	6671(4)	9542(11)	6820(7)	3.7
C4	6860(4)	9016(12)	8128(7)	4.0
C5	7361(5)	10139(16)	9001(9)	6.2
C6	6562(4)	7494(11)	8597(7)	3.3
C7	6080(3)	6482(9)	7824(6)	2.6
C8	5821(4)	4928(9)	8476(6)	2.8
C9	5163(4)	2448(11)	8984(7)	3.7
C10	5037(4)	714(11)	8246(7)	3.8
C11	4296(5)	570(11)	7564(7)	4.1
C12	6065(4)	9213(10)	4672(7)	3.1
C13	2808(5)	6797(14)	7847(11)	5.9
C14	3462(4)	5826(10)	7457(7)	3.5

a) $B_{eq}=4/3[a^2B_{11}+b^2B_{22}+c^2B_{33}+2ab(\cos\gamma)B_{12}+2ac(\cos\beta)B_{13}+2bc(\cos\alpha)B_{23}]$.

Results and Discussion

Crystal Structure of $[Mn_2(L^{3,3})(CH_3COO)_2]$ (4). The ORTEP view of the complex molecule is shown in Fig. 1 together with the numbering scheme. The relevant bond distances and angles are summarized in Table 3.

The crystal consists of one macrocycle $(L^{3,3})^{2-}$, two Mn(II) ions, and two acetate ions. In the centrosymmetric molecule, two Mn ions are bridged by two phenolic oxygens of the macrocycle with Mn–Mn separation of 3.367(1) Å and Mn–O1–Mn′ angle of 103.0(2)°. The Mn–O1 and Mn–O1′ bond distances (2.157(5) and 2.147(4) Å, respectively) and the Mn–N1 and Mn–N2

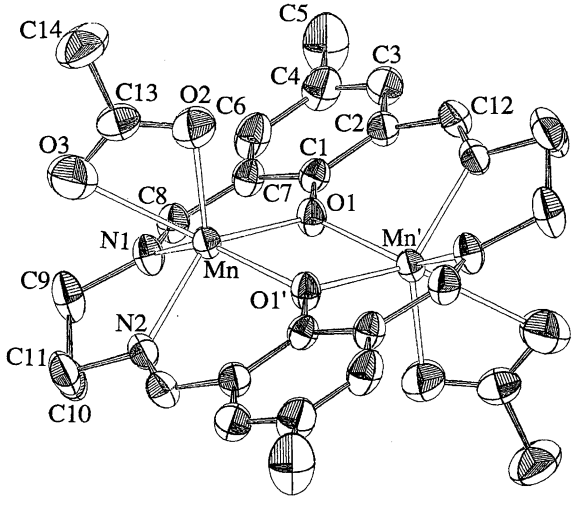

Fig. 1. ORTEP view of **4**.

Table 3. Relevant Bond Distances and Angles of **4**

	Bond distances (Å)		
Mn–O1	2.157(5)	Mn–N1	2.207(5)
Mn–O1′	2.147(4)	Mn–N2	2.194(6)
Mn–O2	2.123(6)		
Mn–O3	2.535(7)	Mn–Mn′	3.367(1)
	Bond angles (deg)		
Mn–O1–Mn′	103.0(2)	O2–Mn–N1	122.4(2)
O1–Mn–O1′	77.0(2)	O2–Mn–N2	115.4(2)
O1–Mn–O2	100.1(2)	O3–Mn–O1′	138.7(2)
O1–Mn–O3	133.1(2)	O3–Mn–N1	81.8(2)
O1–Mn–N1	82.5(2)	O3–Mn–N2	83.3(2)
O1–Mn–N2	141.0(2)	N1–Mn–O1′	136.8(2)
O2–Mn–O1′	98.6(2)	N1–Mn–N2	91.4(2)
O2–Mn–O3	54.7(2)	N2–Mn–O1′	81.8(2)

bond distances (2.207(5) and 2.194(6) Å, respectively) are common for Mn(II) complexes. An acetate ion coordinates bidentately to the metal with Mn–O2 and Mn–O3 bond distances of 2.123(6) and 2.535(7) Å, respectively, to afford a six-coordinate geometry around each Mn. The Mn ion deviates by 0.75 Å from the least-squares plane defined by O1, O1′, N1, and N2 toward the acetate group, and its geometry is much distorted from a regular octahedron as judged from the bond angles about the metal (see Table 3). The macrocycle forms a near coplane where the deviations of the atoms, except for the central carbon (C10) of the lateral chain, from the least-squares plane is less than 0.138 Å. The C10 deviates by 0.684 Å from the least-squares plane. The two Mn ions are situated at different sites with respect to the macrocycle plane. Thus, the least-squares plane defined by Mn, O1, Mn′ and O1′ and the least-squares plane of the macrocycle are slant with a dihedral angle of 19.47°.

The crystal structure of **4** resembles that of a previously reported complex $[Mn_2(L')(CH_3COO)_2]\cdot 2CH_3OH$[22] of a macrocyclic analog $(L')^{2-}$ bearing an OH group on both lateral chains (Mn–Mn 3.34 Å, Mn–O1–Mn 103.6°, Mn–N and Mn–O 2.109—2.217 Å, Mn–O (acetate) 2.281—2.290, deviation of Mn from N_2O_2 plane 0.77 Å). In another complex $[Mn_2(L'')(CH_3COO)]ClO_4$[9] of a macrocyclic analog $(L'')^{2-}$ bearing an OH group on one lateral chain, the acetate group acts as bridge between two dinuclear units affording a five-coordination around each Mn and forming a chain structure. In this complex the deviation of Mn from the basal N_2O_2 plane is 0.61 Å. Evidently, the mismatch between the cavity size and the ionic radius of Mn(II) ion is the main cause for such a large deviation of Mn from the basal N_2O_2 plane.

Physicochemical Properties. The Mn_2(II,II) complexes **1**—**3** were stable in the solid state but were oxidized with molecular oxygen in DMF. The complexes **4** and **5** were air-stable even in DMF and DMSO. Conductivity studies have revealed that **1**—**5** behave as non-electrolytes in DMF, indicating the coordination of the carboxylate groups to the Mn(II) ions. However, the addition of water to the DMF solution resulted in an increase in conductivity. This fact suggests the dissociation of the carboxylate group in aqueous solution. The ν_{as}(COO) and ν_s(COO) modes of the carboxylate group are seen at ca. 1540 and ca. 1400 cm^{-1}, respectively. The separation between the two modes is less than 200 cm^{-1}, indicating the bidentate coordination of the carboxylate group[23] as proved by X-ray crystallography for **4**. Each complex shows an intense absorption band near 380 nm ($\varepsilon \approx 15000$ M^{-1} cm^{-1}) which is assigned to π–π^* transition[24,25] associated with the azomethine linkage. No prominent absorption is seen in the visible region, in accord with the high-spin d^5 electronic configuration of the Mn(II) ions.

The mixed-valence complex **4′** shows a visible band with a moderate intensity at 570 nm in DMSO, which is assigned to a d–d band of the Mn(III) ion. The bidentate coordination of the acetate group must be the case in **4′**, judging from the small separation between the ν_{as}(COO) and ν_s(COO) modes (ca. 150 cm^{-1}). In this complex, the acetate group may coordinate to the Mn(II) and two Br^- ions to the Mn(III),[10] providing a valence-localized dinuclear core.

Magnetic moments of **1**—**5** fall in the range of 5.44—5.92 μ_B (per Mn atom), adding support to the high-spin electronic configuration of the Mn(II) ions. Cryomagnetic studies in the temperature range of 4.2—290 K have suggested a weak magnetic interaction within the molecule. A typical example of $\chi_A T$ vs. T plots is given by trace a in Fig. 2.

The magnetic susceptibility expression for $(S_1=5/2)$–$(S_2=5/2)$ based on the Heisenberg model $H=-2JS_1S_2$

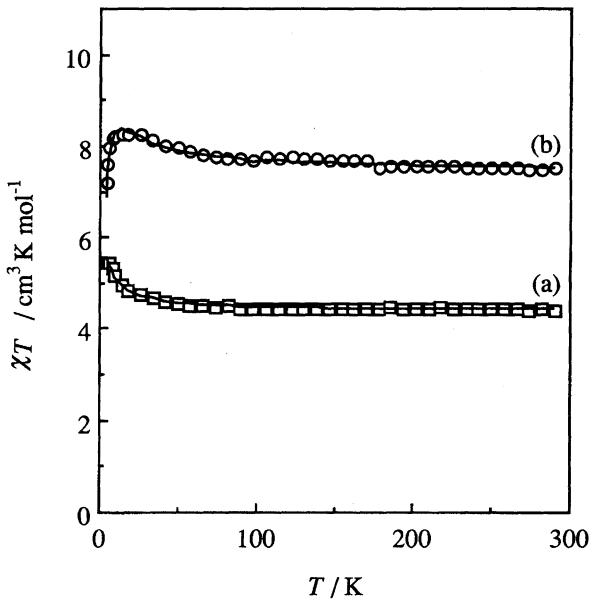

Fig. 2. $\chi \cdot T$ plots for **4** (a; per Mn) and **4′** (b; per two Mn atoms).

is given as follows:

$$\chi_A = \{Ng^2\beta^2/k(T-\theta)\} \times [A/B]$$
$$\text{with } A = \exp(-28J/kT) + 5\exp(-24J/kT) + 14\exp(-18J/kT) + 30\exp(-10J/kT) + 55$$
$$\text{and } B = \exp(-30J/kT) + 3\exp(-28J/kT) + 5\exp(-24J/kT) + 7\exp(-18J/kT) + 9\exp(-10J/kT) + 11 \quad (1)$$

In this equation θ is included as the correction term for inter-dimer interaction and the other symbols have their usual meanings. As is shown by the solid trace in Fig. 2, the cryomagnetic behavior of **4** can be well reproduced by Eq. 1, using the magnetic parameters J=+0.4 cm^{-1}, g=2.00, and θ=−0.8 K. Similarly, the cryomagnetic properties of the other Mn_2(II,II) complexes could be well simulated by this equation. Magnetic parameters and discrepancy factors defined as $R(\chi)=[\sum(\chi_{obsd}-\chi_{calcd})^2/\sum(\chi_{obsd})^2]^{1/2}$ are summarized in Table 4.

The exchange integral J in Mn^1(II)–Mn^2(II) is given by the mean of 25 (=5×5) individual exchange integrals J_{ij} between the ith unpaired electron of Mn^1 and the jth unpaired electron of Mn^2, i.e., $J=\sum J_{ij}/25$. In general, dinuclear Mn(II) complexes show a small J in absolute value, probably because positive and negative J_{ij} contributions to the overall J are comparable. The sign and magnitude of each J_{ij} are sensitive to a small change in dinuclear core structure so that the overall magnetic interaction of **1**—**5** varies from ferromagnetism to antiferromagnetism as seen in Table 4.

The $\chi_M T$ vs. T plots for **4′** are given in Fig. 2 (trace b). The $\chi_M T$ value increases with decreasing temperature up to a maximal value near 14 K, then decreases below this temperature. This trend indicates the operation of a weak ferromagnetic interaction within the molecule. The drop in $\chi_M T$ below 14 K suggests a zero-field splitting of Mn(II) and Mn(III) ions[10] or an inter-dimer antiferromagnetic interaction. Magnetic analyses have been made by the equation (2) for (S_1=5/2)–(S_2=2) based on the isotropic Heisenberg model:

$$\chi_M = \{N\beta^2/4k(T-\theta)\} \times [A/B]$$
$$\text{with } A = g_{1/2}^2 + 10g_{3/2}^2\exp(-3J/kT) + 35g_{5/2}^2\exp(-8J/kT) + 84g_{7/2}^2\exp(-15J/kT) + 165g_{9/2}^2\exp(-24J/kT)$$
$$\text{and } B = 1 + 2\exp(-3J/kT) + 3\exp(-8J/kT) + 4\exp(-15J/kT) + 5\exp(-24J/kT) \quad (2)$$

In this equation $g_{1/2}$, $g_{3/2}$, $g_{5/2}$, $g_{7/2}$, and $g_{9/2}$ mean the g factors of the total spin states S_T=1/2, 3/2, 5/2, 7/2, and 9/2, respectively, and are expressed as $g_{1/2}=(7g-4g')/3$, $g_{3/2}=(13g+2g')/15$, $g_{5/2}=(23g+12g')/35$, $g_{7/2}=(37g+26g')/63$, and $g_{9/2}=(5g+4g')/9$, by the use of local Zeeman splitting factors g and g' of Mn(II) and Mn(III) ions, respectively.[26] As is seen in Fig. 2, the cryomagnetic property of **4′** is well reproduced by Eq. 2. The magnetic parameters obtained by the least-squares fitting are included in Table 4. The result indicates a very weak ferromagnetic interaction between the Mn(II) and Mn(III) ions. For a related mixed-valence Mn_2(II,III) complex[10] a weak antiferromagnetic interaction is reported.

The electrochemical behavior of **1**—**5** was studied in DMF by means of cyclic voltammometry. The numerical data are summarized in Table 5.

The complexes **4** and **5** with $(L^{3,3})^{2-}$ show one quasi-reversible couple at ca. +0.29 V (vs. SCE) which is assigned to the one-electron oxidation process, Mn_2(II,II)/Mn_2(II,III), based on coulometry experiments together with visible and ESR studies for the electrolyzed solution. That is, the electrolyzed solution showed the same visible and ESR spectra as those of the mixed-valence complex **4′** (ESR spectral discussion is given later). It should be mentioned that **4′** shows a similar quasi-reversible couple at +0.24 V.

Each CV of **1** and **2** with unsymmetrical $(L^{2,3})^{2-}$ is not straightforward and contains two reversible couples with similar current heights at close potentials. Our coulometry studies at +0.35 V have revealed one-electron transfer for the two waves altogether. This fact suggests the formation of two Mn_2(II,III) complexes on the electrode. It appears that the two complexes are isomeric with respect to the oxidized metal center; i.e., in one isomer the Mn at the site of the ethylene lateral chain is oxidized (near +0.17 V) and in the other isomer the Mn at the site of the trimethylene chain is oxidized (near +0.29 V).

The complex **3** with $(L^{2,4})^{2-}$ was unstable on the electrode, showing only an anodic peak at +0.41 V.

Catalase-Like Activity. In our recent studies on MnCAT models using μ-phenoxo-bis(μ-carboxylato)dimanganese(II) complexes of Type A and Type B ligands (see Scheme 2),[27,28] a dinuclear *cis*-$\{Mn^{IV}(=O)\}_2$ species has been detected as an active intermediate to disproportionate H_2O_2

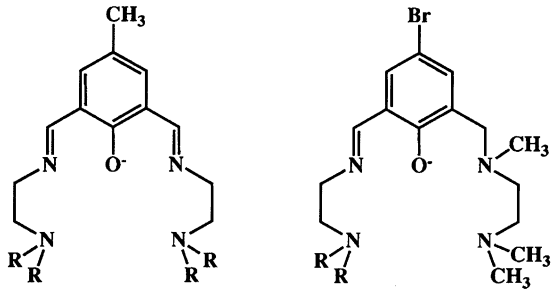

Type A Type B

Scheme 2. Chemical structures of Type A and Type B ligands (R=CH_3, C_2H_5).

Table 4. Magnetic Parameters and Discrepancy Factors of **1**—**5** and **4′**

Complex	J/cm^{-1}	g	θ/K	$R(\chi)\times10^{2a)}$
$[Mn_2(L^{2,3})(CH_3COO)_2]$ (**1**)	+0.3	2.00	−0.8	0.9
$[Mn_2(L^{2,3})(C_6H_5COO)_2]$ (**2**)	+0.3	1.98	−1.2	1.7
$[Mn_2(L^{2,4})(C_6H_5COO)_2]$ (**3**)	−0.6	1.97	0.0	3.1
$[Mn_2(L^{3,3})(CH_3COO)_2]$ (**4**)	+0.4	2.00	−0.8	1.1
$[Mn_2(L^{3,3})(C_6H_5COO)_2]$ (**5**)	+0.4	2.00	−1.2	1.7
$[Mn_2(L^{2,3})(CH_3COO)Br_2]\cdot H_2O$ (**4′**)	+1.0	2.00, 2.02[b)]	−3.4	3.5

a) $R(\chi)=[\sum(\chi_{obsd}-\chi_{calcd})^2/\sum(\chi_{calcd})^2]^{1/2}$. b) g=2.00 for Mn^{2+} and 2.02 for Mn^{3+}.

Table 5. Electrochemical Data for **1**—**5** and **4′** (V vs. SCE)

Complex	E_{pa}/V	E_{pc}/V	$E_{1/2}$[a)]/V
1	+0.25	+0.11	+0.18
	+0.33	+0.25	+0.29
2	+0.21	+0.11	+0.16
	+0.31	+0.25	+0.28
3	+0.41	—	—
4	+0.33	+0.25	+0.29
5	+0.32	+0.23	+0.28
4′	+0.28	+0.20	+0.24

a) $E_{1/2}=1/2(E_{pa}+E_{pc})$.

$(2H_2O_2=2H_2O+O_2)$ along with a less active intermediate $\{Mn^{II}Mn^{IV}(=O)\}$. It is presumed that the *cis*-$\{Mn^{IV}(=O)\}_2$ species is associated with a fast catalytic process by an intramolecular mechanism through the interconversion of *cis*-$\{Mn^{IV}(=O)\}_2$/*cis*-$\{Mn^{III}(OH)\}_2$, whereas $\{Mn^{II}Mn^{IV}(=O)\}$ is associated with slow catalytic process by an intermolecular mechanism through $\{Mn^{II}Mn^{IV}(=O)\}/\{Mn^{II}Mn^{III}(OH)\}$. One noticeable difference in the CAT-like activity between the complexes of Type A ligands and those of Type B ligands is seen in the total amount of evolved dioxygen.[28)] That is, the total amount of dioxygen was theoretical (100%) for the former complexes, whereas it was only 60—70% for the latter complexes. It appears that a side reaction occurs to consume H_2O_2 when a pair of Mn ions are not equivalent in electronic nature. Thus, it is of great interest to examine the CAT-like activity of **1**—**5** in view of the symmetrical or unsymmetrical nature of the macrocycles.

All the Mn_2(II,II) complexes showed catalytic activity for decomposing H_2O_2 in DMF at 0 °C. The time course of O_2 evolution in H_2O_2 decomposition by **1**—**5** at a complex concentration of 2.5×10^{-3} M is given in Fig. 3. The H_2O_2 decomposition rate and the yield of evolved dioxygen vary depending upon the nature of the macrocycles. The effect of the carboxylate group (acetate or benzoate) upon the catalytic activity seems not to be significant. We have noticed that the H_2O_2 decomposition rate highly depends upon the complex concentration and is considerably retarded with decreasing complex concentration (see Fig. 4). In this case, the

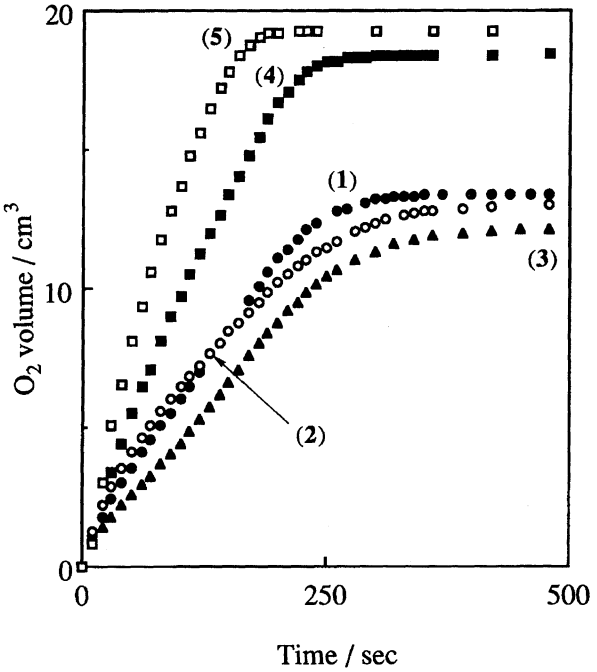

Fig. 3. Time courses of O_2 evolution in H_2O_2 decomposition by **1**—**5**. Conditions: complex, 5 μmol in DMF 2 cm^3; H_2O_2, 1.45 mmol (10.0%, 0.5 cm^3); at 0 °C.

H_2O_2 decomposition reaction was completed within 250 seconds at a complex concentration of 2.5×10^{-3} M but was barely completed after 3900 seconds at 2.5×10^{-4} M. The insert in Fig. 4 is the correlation between the initial O_2-evolution rate (v/$cm^3\,s^{-1}$) and the complex concentration ($[Mn_2]/10^{-3}$ M). A linear relationship between $v^{1/2}$ and $[Mn_2]$ strongly suggests the involvement of a 1:2 adduct of H_2O_2 and the Mn_2(II,II) complex, $[H_2O_2][Mn_2]_2$, in the catalytic H_2O_2 decomposition.

Spectroscopic studies of the reaction mixture were made at 0 °C, and a very rare absorption band with fine structures (ca. 730 cm^{-1}) was observed near 520 nm (Fig. 5). Such an absorption band is characteristic of Mn^{IV}=O complex[27,28)] and can be assigned to the charge-transfer band from O^{2-} to Mn(IV); the fine structures are attributed to the ν(Mn=O) mode imposed on the CT band through vibronic interaction. The CT band appeared after a lag period, first in-

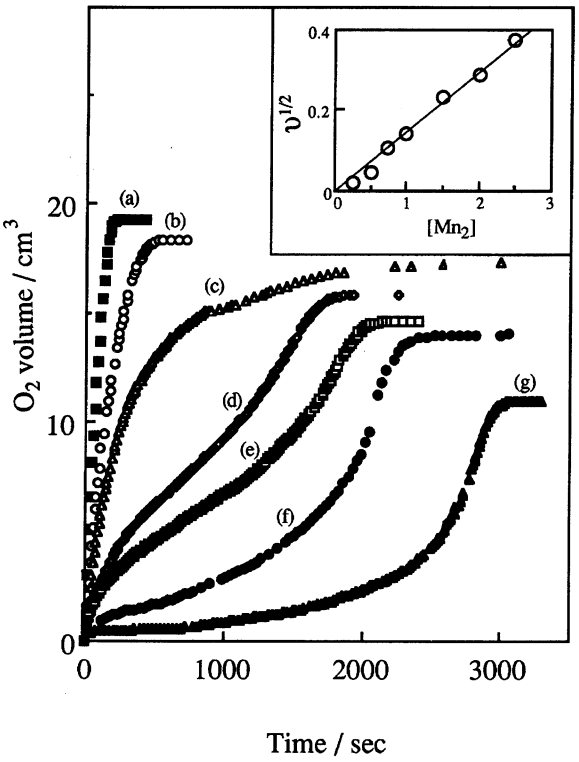

Fig. 4. Time courses of O_2 evolution in H_2O_2 decomposition by **4** at different concentrations (Conditions: total H_2O_2 1.45 mmol, in DMF 2 cm^3, at 0 °C): (a) 2.5×10^{-3} M, (b) 2.0×10^{-3} M, (c) 1.5×10^{-3} M, (d) 1.0×10^{-3} M, (e) 7.5×10^{-4} M, (f) 5.0×10^{-4} M, (g) 2.5×10^{-4} M. The insert shows a linear correlation between the square root of the initial rate of O_2 evolution (v/cm^3 s^{-1}) and the complex concentration ([Mn_2]/10^{-3} M).

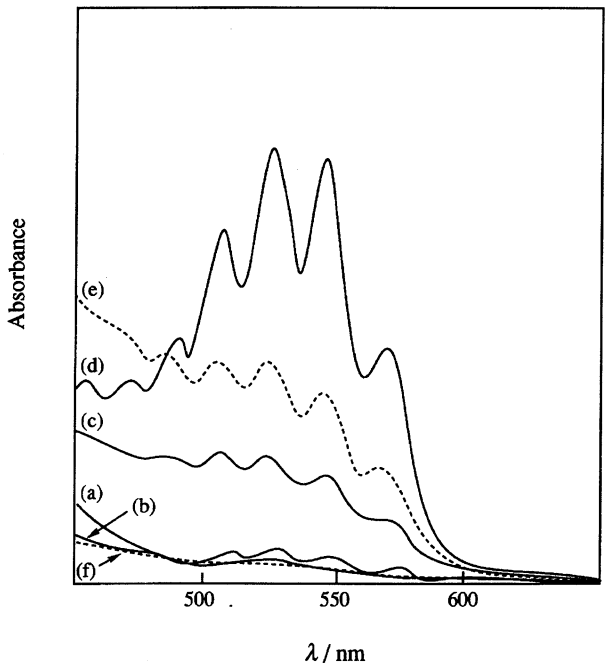

Fig. 5. Time course of visible spectra in H_2O_2 decomposition by **4** at 2.0×10^{-4} M (Conditions: total H_2O_2 1.45 mmol, in DMF 2 cm^3, at 0 °C): (a) after 900 s, (b) 1500 s, (c) 2700 s, (d) 3000 s, (e) 4500 s, (f) 7800 s.

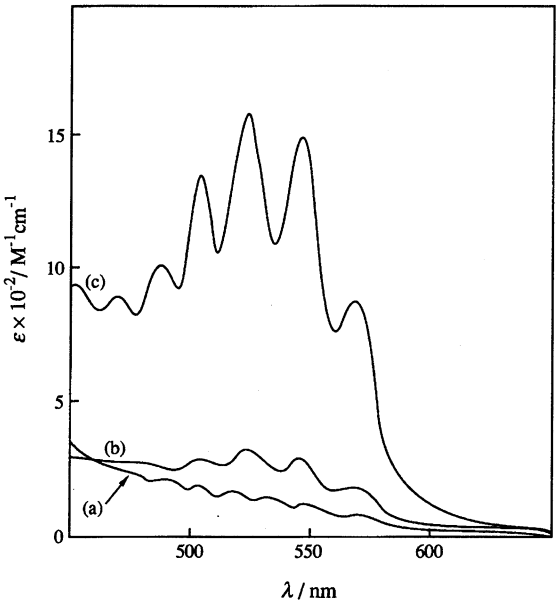

Fig. 6. Visible spectra in H_2O_2 decomposition by **4** at different complex concentrations (Conditions: total H_2O_2 1.45 mmol, in DMF 2 cm^3, at 0 °C): (a) 1.0×10^{-3} M, (b) 5.0×10^{-4} M, (c) 2.5×10^{-4} M. The spectrum with the highest CT band in the time course at each complex concentration is given.

creased and then decreased its intensity, and finally disappeared. It should be emphasized that the time course of the CT band is in good accord with the time course of the O_2 evolution when compared at the same complex concentration; the CT band reached a maximum when O_2 was most violently evolved. This fact strongly suggests the involvement of a Mn^{IV}=O complex in the catalytic decomposition of H_2O_2. It should be noted that the CT band is observed prominently at a low complex concentration as seen in Fig. 6. In this case, the ν(Mn=O) vibration mode of the CT band was barely seen at a complex concentration of 1.0×10^{-3} M but was not seen at higher concentration. It is presumed that the Mn^{IV}=O species has a long life time at low complex concentration.

The reaction mixtures were submitted to ESR spectroscopic studies at liquid nitrogen temperature to observe a 6-line hypefine structure and a 10-line structure of weaker intensity for all the cases, irrespective of complex concentration. The ESR spectrum for the reaction mixture with **4** is shown in Fig. 7. Exactly the same ESR spectrum was obtained for the Mn_2(II,III) complex of **4**, prepared by coulometry, and for the mixed-valence complex **4′** (see Fig. 7). We have studied the time course of the ESR spectra in comparison with that of the CT band and confirmed that the ESR signals appear prior to the CT band and retain their intensity until all H_2O_2

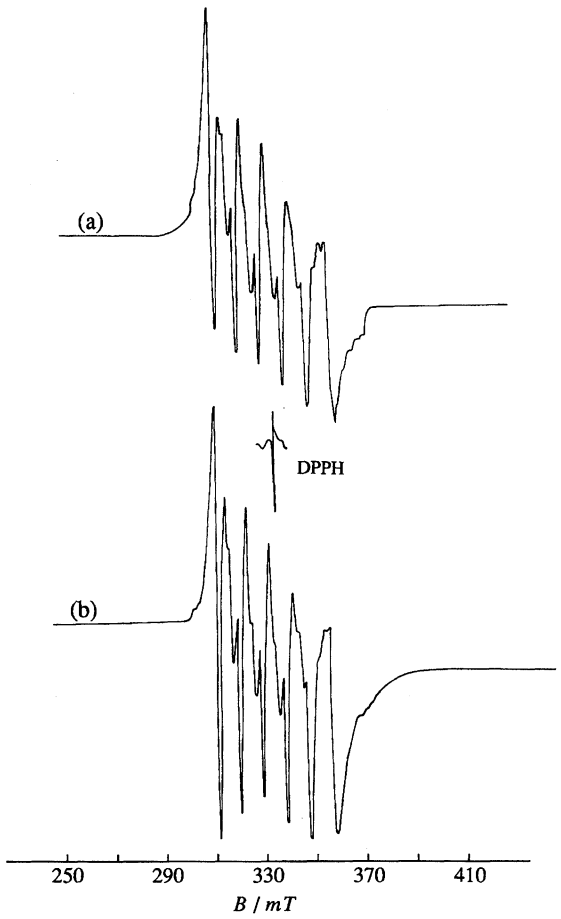

Fig. 7. ESR spectra for the reaction mixture with **4** (a) and for the mixed-valence complex **4′** (b).

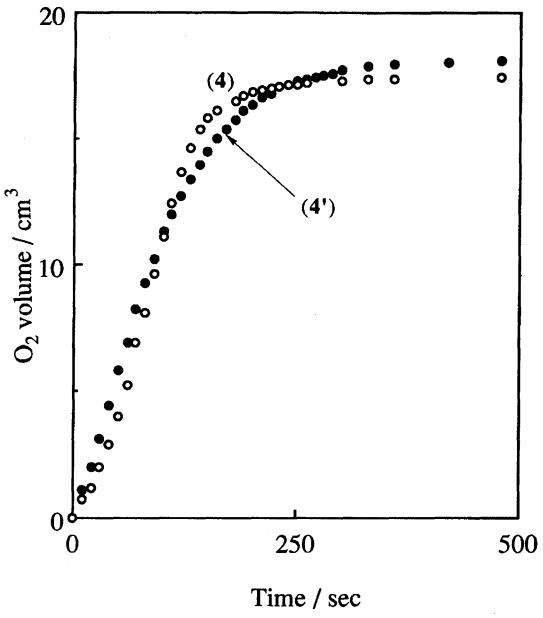

Fig. 8. Catalytic O_2 evolution profiles in H_2O_2 decomposition by **4** and **4′**. Conditions: complex, 2.5 μmol in DMSO 2 cm^3; H_2O_2, 1.45 mmol (10.0%, 0.5 cm^3); at 20 °C.

is decomposed. Evidently, the ESR signals arise from a Mn_2(II,III) complex formed in the H_2O_2 decomposition reaction. Very similar ESR spectra have been reported for a related Mn_2(II,III) complex.[10] Chang et al.[10] have assigned the strong 6-line structure to the $\Delta M_I=0$ spin-allowed transitions and the weak 10-line structure to the $\Delta M_I=1$ spin-forbidden transitions of Mn(II) ion. Such hyperfine structures may be observed when Mn(II) and Mn(III) ions are effectively uncoupled, in accord with a weak magnetic interaction in **4′**.

In order to see if the Mn_2(II,III) complex is involved in the catalytic H_2O_2 decomposition process, we have compared **4** and **4′** in the CAT-like activity in DMSO. The use of DMSO as the solvent was due to the low solubility of **4′** in DMF. As seen in Fig. 8, the two complexes gave very similar O_2-evolution profiles in H_2O_2 decomposition. This may be taken as a good indication that the Mn_2(II,III) is indeed involved as an active form in the catalytic process. It is generally believed that Mn_2(II,III) is not involved in catalysis of native MnCAT, but this has not been thoroughly studied.[29]

The active Mn_2(II,III) species may be best described as $Mn^{II}Mn^{III}$(OH) and thence its oxidized Mn_2(II,IV) species as $Mn^{II}Mn^{IV}$(=O).[27] The latter formulation is consistent with the observed CT band with ν(Mn=O) vibration modes. At this stage, a question arises concerning why the $Mn^{II}Mn^{IV}$(=O) complex does not show ESR signals. If the magnetic exchange between the Mn(II) and Mn(IV) ions is weak, ESR signals like those in Fig. 7 may be observed along with signals of Mn(IV). If the magnetic exchange is significant, both Mn(II) and Mn(IV) ions are hardly detected by ESR spectroscopy owing to fast spin relaxation. No Mn(II)Mn(IV) complexes have been reported so far but a trinuclear Cr_2Mn complex with di(hydroxo)-bridged Mn(II)Cr(III) unit, isoelectronic with Mn(II)Mn(IV), is available.[30] The magnetic interaction in this complex is moderately antiferromagnetic, suggesting the broadening of the ESR signals in the $Mn^{II}Mn^{IV}$(=O) complex. It may also be the case that the amount of the $Mn^{II}Mn^{IV}$(=O) complex formed in the reaction mixture is very small relative to the $Mn^{II}Mn^{III}$(=OH) complex, judging from the apparent intensity of the CT band ($\varepsilon\approx1500$ M^{-1} cm^{-1} at best).

Based on the above results and together with our previous studies,[27,28] the mechanistic scheme of H_2O_2 decomposition with **1**—**5** is discussed. The X-ray crystallography of **4** has revealed the C_2 symmetric core structure with two labile acetate groups trans to each other with respect to the macrocyclic coplane. For this reason, the chelating interaction of peroxide ion with two Mn ions within the molecule is impossible. The only possible interaction is the intermolecular bridge {$Mn^{II}Mn^{II}$–O–O–$Mn^{II}Mn^{II}$}, in accord with the kinetic result for **4** (Fig. 4), from which the mixed-valence complex {$Mn^{II}Mn^{III}$(OH)} can be derived by the two-

electron transfer from two Mn(II) ions to the bridging O_2^{2-}. A stable $Mn^{III}(OH)$ complex is known[31] which shows a CAT-like activity, probably through the cycle $\{Mn^{IV}(=O)\}/\{Mn^{III}(OH)\}$.[28] If the cycle between the oxidized and reduced forms in H_2O_2 disproportionation is fast, neither of the two forms can be detected owing to their short life time. When the cycle is slowed, either or both of the forms may have a sufficiently long life time to be detected by any spectroscopic method. In the catalytic H_2O_2 decomposition using the Mn_2 complexes of Type A and Type B ligands, the oxidized form $\{Mn^{IV}(=O)\}_2$ could be detected by visible spectroscopy and mass spectrometry.[27,28] In the present case, the cycle $Mn^{II}Mn^{IV}(=O)/Mn^{II}Mn^{III}(OH)$ is slowed at low complex concentration at 0 °C, allowing us to detect the $Mn^{II}Mn^{IV}(=O)$ complex by visible spectroscopy. The cycle becomes faster with increasing complex concentration, making it more difficult to observe the characteristic CT band of the $Mn^{II}Mn^{IV}(=O)$ complex. The involvement of the $Mn^{II}Mn^{III}(=OH)$ complex in the catalytic cycle, irrespective of the complex concentration, is evident from the ESR spectra determined at liquid nitrogen temperature.

The yield of evolved dioxygen varies depending upon both the nature of the macrocycles and the complex concentration used as the catalyst (see Table 6). At high complex concentration, the yield is nearly theoretical (100%) for **4** and **5** with symmetrical $(L^{3,3})^{2-}$ whereas it is always lower than 100% for **1**—**3** with unsymmetrical $(L^{2,3})^{2-}$ and $(L^{2,4})^{2-}$. In **1**—**3**, the two metal ions are not equivalent in electronic nature so that two different interaction modes of H_2O_2 with two Mn centers are possible, i.e., $Mn^BMn^A\cdots O\text{–}O\cdots Mn^AMn^B$ and $Mn^AMn^B\cdots O\text{–}O\cdots Mn^AMn^B$. The latter interaction of H_2O_2 with two non-equivalent Mn centers may lead, more or less, to a heterolytic fission of the O–O bond of hydrogen peroxide, though the detailed mechanism remain to be studied further. At low complex concentration, the yield of dioxygen decreases in all cases. The $Mn^{II}Mn^{IV}(=O)$ and $Mn^{II}Mn^{III}(OH)$ complexes may form a 1 : 1 adduct with H_2O_2 at low complex concentration, and the 1 : 1 adduct may cause a heterolytic fission of the O–O bond. Thus, this work adds support to the significance of an equivalent pair of Mn ions in a MnCAT-like reaction, irrespective of intramolecular or intermolecular mechanism.

Table 6. Yields of Evolved Dioxygen (%) in H_2O_2 Decomposition by **1**—**5** at Different Complex Concentrations

Complex	Complex concentration/M		
	0.25×10^{-3}	2.5×10^{-3}	4.0×10^{-3}
1	49	74	—
2	55	72	81
3	56	67	72
4	58	100	—
5	57	100	100

Conditions: H_2O_2 (10.0%, 0.5 cm^3) and a complex in DMF (2 cm^3) at 0 °C.

This work was supported by a Grant-in-Aid for Scientific Research on Priority Area No. 03241105 and a Grant-in-Aid for Encouragement of Yound Scientists No. 06740511 from the Ministry of Education, Science and Culture.

References

1) D. E. Fenton and H. Ōkawa, "Perspectives on Bioinorganic Chemistry," ed by R. W. Hay, J. R. Dilworth, and K. B. Nolan, JAI Press (1993), Vol. 2, pp. 81—138.

2) P. A. Vigato, S. Tamburini, and D. E. Fenton, *Coord. Chem. Rev.*, **106**, 25 (1990).

3) J. D. Lamb, R. M. Izatt, J. J. Christensen, and D. J. Eatough, "Coordination Chemistry of Macrocyclic Compounds," ed by G. A. Melson, Plenum Press, New York (1979), p. 145.

4) J. F. Endicott and B. Durham, "Coordination Chemistry of Macrocyclic Compounds," ed by G. A. Melson, Plenum Press, New York (1979), p. 393.

5) N. H. Pilkington and R. Robson, *Aust. J. Chem.*, **23**, 2225 (1970).

6) H. Ōkawa and S. Kida, *Inorg. Nucl. Chem. Lett.*, **7** 751 (1971); H. Ōkawa and S. Kida, *Bull. Chem. Soc. Jpn.*, **45**, 1759 (1972).

7) M. Tadokoro, H. Ōkawa, N. Matsumoto, M. Koikawa, and S. Kida, *J. Chem. Soc., Dalton Trans.*, **1991**, 1657; M. Tadokoro, H. Sakiyama, N. Matsumoto, M. Kodera, H. Ōkawa, and S. Kida, *J. Chem. Soc., Dalton Trans.*, **1992**, 313.

8) H. Ōkawa, J. Nishio, M. Ohba, M. Tadokoro, N. Matsumoto, M. Koikawa, S. Kida, and D. E. Fenton, *Inorg. Chem.*, **32**, 2949 (1993).

9) D. Luneau, J.-M. Savariault, P. Cassoux, and J.-P. Tuchagues, *J. Chem. Soc., Dalton Trans.*, **1988**, 1225.

10) H.-R. Chang, S. K. Larsen, P. D. W. Boyd, C. G. Pierpont, and D. N. Hendrickson, *J. Am. Chem. Soc.*, **110**, 4565 (1988).

11) R. M. Fronko, J. E. Penner-Hahn, and C. J. Bender, *J. Am. Chem. Soc.*, **110**, 7554 (1988); G. S. Allgood and J. J. Perry, *J. Bacteriol.*, **168**, 563 (1986).

12) A. Willing, H. Follmann, and G. Auling, *Eur. J. Biochem.*, **170**, 603 (1988).

13) B. S. Cooperman, A. A. Baykov, and R. Lahti, *TIBS*, **17**, 262 (1992); N. Y. Chiradze, I. P. Kuranova, N. A. Veirskaya, A. V. Teplyakov, K. Wilson, B. V. Srokopytov, E. G. Harutyunyan, and W. Hohne, *Kristallografiya*, **36**, 128 (1991).

14) R. S. Reczkowski and D. E. Ash, *J. Am. Chem. Soc.*, **114**, 10992 (1992).

15) H. L. Carrell, J. P. Glusker, V. Burger, F. Manfre, D. Tritsch, and J. F. Biellmanh, *Proc. Natl. Acad. Sci. U. S. A.*, **86**, 4440 (1989); C. A. Collyer, K. Henrick, and D. M. Blow, *J. Mol. Biol.*, **212**, 211 (1990).

16) E. A. Boudreaux and L. N. Mulay, "Theory and Applications of Molecular Paramagnetism," Wiley, New York (1976), pp. 491—494.

17) D. A. Denton and H. Suschitzky, *J. Chem. Soc.*, **1963**, 4741.
18) "International Tables for X-Ray Crystallography," Kynoch Press, Birmingham (1974), Vol. 4.
19) S. Kawano, *Rep. Comput. Cent., Kyushu Univ.*, **16**, 113 (1983).
20) T. Sakurai and K. Kobayashi, *Rep. Inst. Phys. Chem. Res. Jpn.*, **55**, 69 (1979).
21) C. K. Johnson, "Rep. No. ORNL3794," Oak Ridge National Laboratory, Oak Ridge, TN (1965).
22) A. J. Downard, V. McKee, and S. S. Tandon, *Inorg. Chim. Acta*, **173**, 181 (1990).
23) G. B. Deacon and R. J. Phillips, *Coord. Chem. Rev.*, **33**, 227 (1980).
24) B. Bosnich, *J. Am. Chem. Soc.*, **90**, 627 (1968).
25) R. S. Downing and F. L. Urbach, *J. Am. Chem. Soc.*, **91**, 5977 (1969).
26) O. Kahn, *Struct. Bonding (Berlin)*, **68**, 89 (1987).
27) H. Sakiyama, H. Ōkawa, and R. Isobe, *J. Chem. Soc., Chem. Commun.*, **1993**, 882; H. Sakiyama, H. Ōkawa, and M. Suzuki, *J. Chem. Soc., Dalton Trans.*, **1993**, 3823.
28) C. Higuchi, H. Sakiyama, H. Ōkawa, R. Isobe, and D. E. Fenton, *J. Chem. Soc., Dalton Trans.*, **1994**, 1097.
29) P. J. Pessiki and G. C. Dismukes, *J. Am. Chem. Soc.*, **116**, 898 (1994).
30) K. M. Corbin, J. Glerup, D. J. Hodgson, M. H. lynn, K. Michelsen, and K. M. Nielsen, *Inorg. Chem.*, **32**, 18 (1993).
31) D. M. Eichhorn and W. H. Armstrong, *J. Chem. Soc., Chem. Commun.*, **1992**, 85.